ADVANCED MATERIALS INTERFACES
www.advmatinterfaces.de

Three-Dimensional Graphene Composite Macroscopic Structures for Capture of Cancer Cells

*Shengyan Yin, Yun-Long Wu, Benhui Hu, Yu Wang, Pingqiang Cai, Chek Kun Tan, Dianpeng Qi, Liyan Zheng, Wan Ru Leow, Nguan Soon Tan, Shutao Wang, and Xiaodong Chen**

Graphene has attracted tremendous interest in the fields of materials science and biomedicine due to its extraordinary physiochemical properties, such as mechanical strength, large surface area, biocompatibility and chemically stability.[1–6] Significant progress has been made in the use of graphene for bio-related applications, including biosensing through graphene-quenched fluorescence, graphene-assisted cell imaging, and graphene-based nanocarrier for drug delivery and cancer therapy.[7,8] However, the development of graphene-based biomaterials/devices for applications, such as biological detection and tissue engineering, is still in its infancy, requiring the rational design and assembly of graphene or its derivatives to achieve novel functions.[9,10] Further integration of the widely available graphene sheets as two-dimensional (2D) nanoscale building blocks, into three-dimensional (3D) macroscopic assemblies and ultimately into a functional system is essential to extend its biomedical applications.[9,11–13] Recently, we reported that the graphene-based free standing honeycomb films synthesized via the "on water spreading" method exhibited superior broad spectrum antibacterial activity, which provided a low-cost facile strategy for the creation of such graphene assemblies and may serve as a useful architecture for promising biomedical applications.[14]

Circulating tumor cells (CTCs) are cells that have shed into the vasculate from a primary tumor and circulate in the blood vessel,[15,16] and facilitate the spread of carcinomas.[17,18] The detection and isolation of CTCs have recently become a topic of interest in cancer research.[19,20] To date, several technologies, such as magnetic separation by capture-agent coated magnetic beads,[21] mechanical separation to isolate CTCs by size difference,[22–24] and microfluidics-based cell capture through enhancing cell-substrate contact frequency,[25–31] have been developed for specific recognition and capture of targeted CTCs. Recently, a silicon nanowire substrate coated with antibody targeting epithelial cell adhesion molecules (i.e., EpCAM), has been successfully utilized to isolate EpCAM-positive CTCs with high capture efficiency.[10,32] The mechanism of this relies on the enhanced local topographic interactions between the substrate and nanoscale components of the cellular surface (i.e., microvilli and filopodia).[32–36] Such systems allow for considerable increase in the contact frequency between substrate and target cells, thus enhancing the filtration and CTC-capture efficiency,[37–41] and enabling a variety of increasingly sensitive and reproducible techniques for CTC detection and therapy.[30,32,42,43]

Herein, we report a 3D hierarchical nanostructured graphene platform that uniquely combines microporosity with immunoaffinity-driven cancer cell-capture nanostructure by integrating 1) ZnO nanorod array grown on 3D free-standing graphene foam, and 2) anti-EpCAM coating for recognizing/capturing EpCAM-expressing cancer cells. The advantage of this novel composite structure lies in its high density of ZnO nanorods, which endows it with the ability to increase cell-substrate contact frequency within 3D space, as well as its microporosity, which allows normal red blood cells to travel through but selectively captures CTCs due to the anti-EpCAM modification. This is the first report describing the use of newly engineered 3D free-standing graphene foam with potential application for cancer cell capture. The graphene foam was chosen as the macro-scaffold due to its chemically inertness, mechanical strength, as well as the biocompatibility and antibacterial property.[11] In order to increase CTC capture efficiency, ZnO nanorods with excellent biocompatibility[44,45] and easy modification with the antibody were employed as the nanopillar array standing on the graphene foam. The resultant nanometer-scale ZnO nanorods topography on the graphene foam substrate was demonstrated to show enhanced interactions with cells, as the ZnO nanorods significantly increased the local ratio of cell affinity molecules to cells. Our results show that CTC-capture yields of more than 80% can be achieved through the use of our fabricated 3D graphene composite macroscopic structures.

Dr. S. Yin, Dr. Y.-L. Wu, B. Hu, Y. Wang, P. Cai, Dr. D. Qi, Dr. L. Zheng, W. R. Leow, Prof. X. Chen
School of Materials Science and Engineering
Nanyang Technological University
50 Nanyang Avenue, Singapore, 639798, Singapore
E-mail: chenxd@ntu.edu.sg
Dr. Y.-L. Wu
School of Pharmaceutical Sciences
Xiamen University
Xiamen, Fujian, P. R. China, 361102, China
Dr. C. K. Tan, Prof. N. S. Tan
School of Biological Sciences
Nanyang Technological University
60 Nanyang Drive, Singapore, 637551, Singapore
Prof. N. S. Tan
Institute of Molecular and Cell Biology (IMCB)
A*STAR, 61 Biopolis Drive, Proteos Building, Singapore
138673, Singapore
Prof. S. Wang
Institute of Chemistry Chinese Academy of Sciences
2 Zhongguancun North First Street
Beijing, P. R. China, 100190, China

DOI: 10.1002/admi.201300043

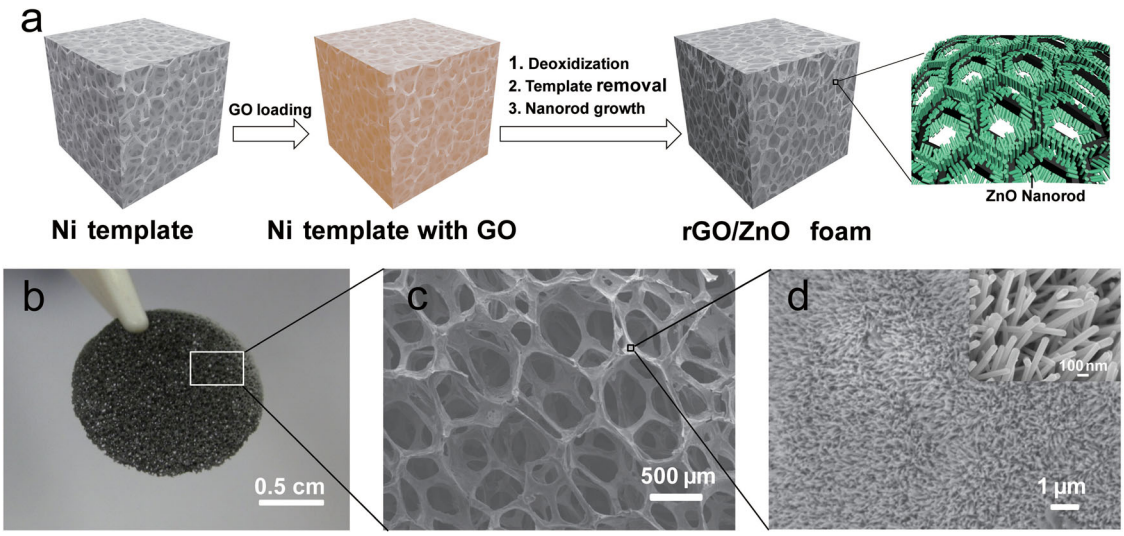

Figure 1. Schematic drawing and configuration of the formed free-standing reduced graphene oxide composite foam (rGO/ZnO foam). a) Schematic drawing of the preparation of the free-standing rGO/ZnO foam; b) Photograph of self-supporting rGO/ZnO foam; c) SEM image of free-standing rGO/ZnO foam; and d) SEM image of the ZnO nanorods on the rGO/ZnO foam (inset: magnified ZnO nanorods).

The fabrication of this novel 3D hierarchical graphene cell-captured foam (rGO/ZnO foam) is illustrated in **Figure 1**a. Firstly, a piece of nickel foam (NF) (1.0 mm thick) was immersed in a suspension of GO (2.2 mg/mL), and the resultant GO/NF was then dried under the room temperature. During the drying process, the GO sheets were deposited on the framework of the nickel foam surface. The resultant GO/NF composite foam was further reduced by the N_2H_4 vapor to form rGO film on the surface of the nickel foam. The removal of Ni foam from the rGO/NF was then performed by immersing the rGO/NF in hydrochloric acid (2 mol/L) at 80 °C for 10 h, before keeping it at room temperature overnight. It is noted that the resultant rGO foam is self-supporting after the removal of the nickel foam. This is because after the GO was reduced to rGO, the strong interactions of adjacent graphene sheets in the graphene film ensured the firmness of the rGO network, which would keep the graphene foam self-supporting. Upon obtaining the self-supporting graphene foam, we deposited ZnO nanorods on its surface through an aqueous solution growing method (see experiment section), and the rGO/ZnO foam remained self-supporting after the process (Figure 1b). The scanning electron microscopy (SEM) image of rGO/ZnO foam surface clearly showed that the rGO/ZnO foam had a 3D inter-penetrating porous structure with pore sizes in the range of hundreds of micrometers (Figure 1c), which successfully preserved the structure of the nickel foam. The micropores allow large entities such as some kinds of cells to pass through which render it suitable for cell separation. The magnified SEM image in Figure 1d showed that the graphene foam surface was modified with densely packed ZnO nanorods of diameters between 40–60 nm and lengths within 1–2 μm. In addition, XRD data (Figure S1) confirms that the ZnO nanorods are highly pure crystals of the hexagonal wurzite-type.

In order to improve the CTC capture efficiency, we further coated this novel 3D rGO/ZnO foam with a cancer-cell capture agent (an epithelial cell adhesion molecule antibody, anti-EpCAM) using a method similar to previous reports.[32] Generally speaking, after growth of the ZnO nanorods on the graphene scaffold, a photocrosslinker was affixed onto the ZnO substrate via photochemical reaction. The photocrosslinker, sulfosuccinimidyl 6-(4′-azido-2′-nitrophenylamino) hexanoate (sulfo-SANPAH) contained at one end a succinimidyl ester group, which reacted with ~NH_2 group of streptavidin in order to attach it onto the surface of the rGO/ZnO foam. Biotinylated anti-EpCAM was then introduced onto the streptavidin-coated substrate prior to the cell-capture experiment (as shown in **Figure 2**a). It was deduced that the final hierarchical 3D graphene foam containing ZnO nanorods coated with CTC capture antibody (anti-EpCAM) would provide a higher local ratio of cell affinitive nanopillars to targeted cells than the planar surface in the following cell capture process, and thus exhibit outstanding cell-capture efficiency when employed to isolate viable CTCs from artificial-blood samples.

To test the cell-capture performance of the rGO/ZnO foams with anti-EpCAM coating (rGO/ZnO/anti-EpCAM foam), an EpCAM-positive breast-cancer cell line was employed as a model system. Specifically, the MCF7 breast cancer cells[46] in cell culture medium (Dulbecco's modified Eagle's medium, DMEM) was used. The MCF7 cell suspension (10^5 cells/mL, 0.3 mL) was introduced onto the rGO/ZnO/anti-EpCAM foam (1.5 cm in diameter), which was then placed in a commercial cell chamber slide (2.2 cm × 2.2 cm) and kept in an incubator (5% CO_2, 37 °C) for 30 min. As control experiments, the flat glass substrate, the pure rGO foam produced through same modified process, and the rGO/ZnO foam without anti-EpCAM coating were also examined in parallel. After rinsing, fixing, and nuclear staining with 4′, 6-diamidino-2-phenylindole (DAPI), a blue fluorescence, the substrate-immobilized cells were imaged and counted using a fluorescence microscope.

Then the cell capture abilities on the different substrates were compared. From Figure 2c, the clear blue dots represented cells on focal plane and indistinct dots represented

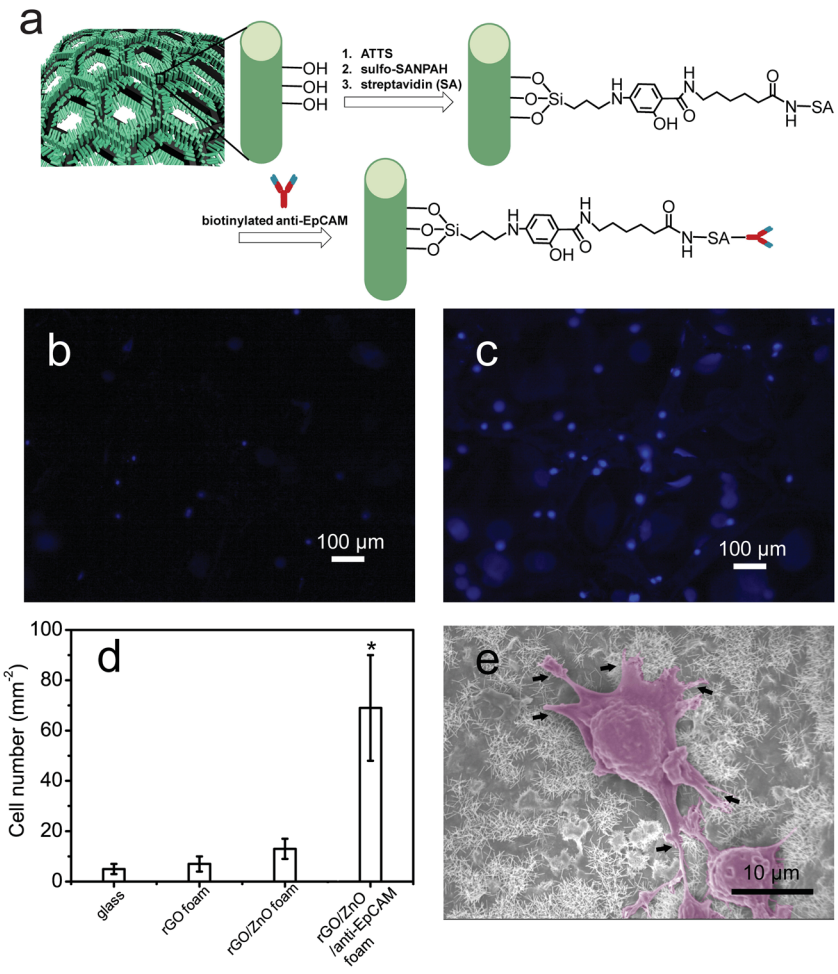

Figure 2. a) Grafting of biotinylated epithelial-cell adhesion-molecule antibody (anti-EpCAM) onto free-standing rGO/ZnO foam; fluorescence micrographs of b) rGO/ZnO foam, and c) rGO/ZnO/anti-EpCAM foam which MCF7 cells were captured (staining with 4′, 6-diamidino-2-phenylindole (DAPI), blue fluorescence); d) the cell capture number on the different substrates (*P<0.05 compared with pure rGO foam, n = 5); and e) SEM image of MCF7 cell being captured on rGO/ZnO/anti-EpCAM foam.

cells at different focal planes that are out of focus (Figure S3), from which it can be deduced that the rGO/ZnO foam comprises vast 3D space for CTC capture. The experimental results demonstrated that the rGO/ZnO/anti-EpCAM foam (Figure 2c) captured a significantly large amount of cells, as compared to the rGO/ZnO foam without antibody coating (Figure 2b). As shown in Figure 2d, the cell capture yield showed a slow increase in the sequence: glass, rGO/foam, rGO/ZnO foam, suggesting that the enhanced local topographic interactions between the substrate and the cellular surface with the increasing surface area. However, only rGO/ZnO/anti-EpCAM foam showed a significantly enhanced cell capture ability, i.e. a capture of up to 13 times more cells than the flat glass substrate (Figure S4a), about 10 times more cells than the pure rGO foam (Figure S4b), and about 5 times more cells than the rGO/ZnO foam (Figure 2b). Thus, the successful modification of the substrate with an antibody that targeted epithelial cell adhesion molecules was indispensable for high yield cell capture. Although glass and rGO foam substrates were treated with anti-EpCAM coating via same process, they still exhibited low cancer cell capture efficiency. The above results suggested that the largely enhanced cell capture ability of the rGO/ZnO/anti-EpCAM foam was the combined result of the antibody modified nanopillars with increased cell-substrate contact frequency and the 3D graphene foam with microporosity. We also used SEM to study the morphologies of the substrate-immobilized cells, by fixing the samples with 4% glutaraldehyde followed by dehydration treatment.[47] The typical morphologies of cells captured on the rGO/ZnO/anti-EpCAM foam clearly displayed the fully outspread pseudopodia attached to the ZnO nanorods (Figure 2e), indicating the sufficient contact and efficient adhesion between cells and substrate. The summation of these results provided solid evidence that our 3D rGO/ZnO/anti-EpCAM foam yielded largely enhanced capture efficiency through the modification of nanopillars, which provided a higher local ratio of cell affinitive antibody to targeted cells.

As both graphene and ZnO possess good biocompatibility[4,45] and electrical properties, the rGO/ZnO/anti-EpCAM foam is highly suitable for use as a CTCs detector. To test this hypothesis, a rGO/ZnO/anti-EpCAM foam device was first put on a glass substrate (as shown in **Figure 3**a). The uncoated graphene area was then passivated with Tween 20, to prevent non-specific binding between substrate and the cells. Finally, the rGO/ZnO/anti-EpCAM foam was incubated with 10^5 cells/mL of MCF7 for CTC detection. As shown in Figure 3b, the relative resistance of the device increases with time due to the gradual increase in the number of EpCAM-positive MCF7 cells captured by the rGO/ZnO/anti-EpCAM foam. This may be ascribed to

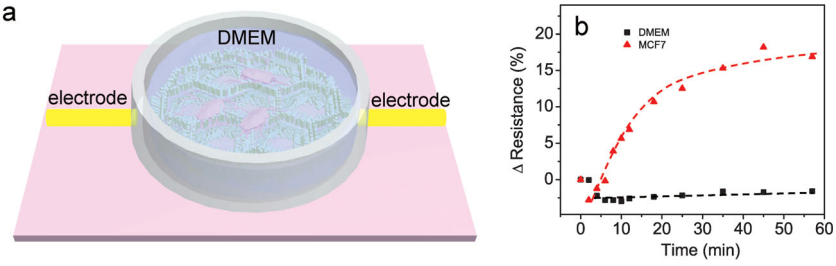

Figure 3. a) Schematic drawing of electrical measurements of rGO/ZnO/anti-EpCAM foam during CTCs capturing. b) Relative resistance change of rGO/ZnO/anti-EpCAM foam versus time following in DMEM (black, square), and MCF7 cell in DMEM (red, triangle) at 37 °C and 5% CO_2.

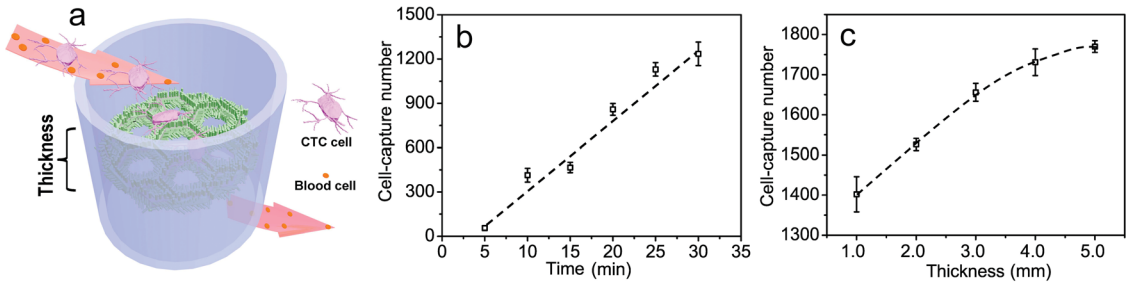

Figure 4. Quantitative evaluation of cell-capture yields. a) Schematic drawing of targeted CTC capture from blood sample; plots of cell-capture number with b) different capture time ranging from 5 min to 30 min (foam thickness: 1 mm) and c) different foam thickness ranging from 1.0 mm to 5.0 mm (incubation time: 30 min).

the presence of MCF7 cells on the foam surface, producing an elevation in electrode impedance that increases with cell number and the degree of cell adhesion.[48] This implies that our rGO/ZnO/anti-EpCAM foam will give useful applications in CTC capture, detection, and diagnosis.

Based on the above experimental results, we believe that this 3D graphene composite foam, compared to the current microfluidic-based devices,[30] has the following advantages: i) it is an easily fabricated CTC capture device, ii) its free-standing 3D architecture increases the cell contact frequency in all directions, and hence iii) no vertical flow of CTC samples needs to be induced in order to ensure complete contact of the samples with the substrate, unlike current chaotic mixing channels.[30] In order to further verify this hypothesis, we employed this 3D graphene composite foam as a syringe filter to test the capture efficiency of this novel but facilely constructed device, as shown in **Figure 4**a and Figure S5. As shown in Table S1, the number of red blood cells, white blood cells and platelets in fresh blood does not change significantly before and after passed through the rGO/ZnO/anti-EpCAM foam.

The performance of this novel 3D rGO/ZnO/anti-EpCAM foam was further investigated through the use of artificial blood samples (Figure 4a), based on different sample incubation time and tunable foam thickness. A series of artificial CTC blood samples with volume of 1 mL was prepared by spiking mouse blood with MCF7 cells labeled by the red fluoresence CellTracker™, at densities within 2000–2200 cells/mL in blood. Prior to cell capture studies, we confirmed EpCAM expression levels on the cell lines using flow cytometry. In the first study, the cell-capture performances of the rGO/ZnO/anti-EpCAM foam (1.5 cm in diameter) with fixed 1 mm thickness with different incubation times was examined using EpCAM-positive cancer cell lines (MCF7) (Figure 4b). Since shrinkage of the blood cells were observed with treatment time longer than 30 min in our experimental conditions, the times of study were chosen to be between 5 min and 30 min. Interestingly, we noticed that the number of substrate-immobilized cells was less than 50 within the initial 5 min, but the amount of captured cells increased linearly with increasing incubation time (Figure 4b). At the incubation time of 30 min, the cell-capture yield of rGO/ZnO/anti-EpCAM foam was able to reach up to 58%. In the second study, in order to investigate the effect of the rGO/ZnO/anti-EpCAM foam thickness on the cell-capture yield, we performed cell-capture experiments with rGO/ZnO/anti-EpCAM foams of thicknesses 1, 2, 3, 4, and 5 mm, respectively. The minimum foam thickness required for optimal capture yield is required to be compatible with cell-protrusion lengths of tumor cells.[49] In our case, the size of cancer cell is about 20 µm in diameter, which is much smaller than the thickness of the foam used. As shown in Figure 4c, the number of captured cells increased with increasing foam thickness. This observation suggested that the enhanced 3D local topographic interactions is due to the synergistic interplay of various characteristics of the rGO/ZnO/anti-EpCAM foam, including but not limited to thickness.[50] When thickness of the anti-EpCAM-coated rGO/ZnO foam reaches 5 mm, the cell capture yield was more than 80%, indicating that our approach showed vastly improved capture yield compared to those observed for the commercialized technology (average yield: 37%).[51] This implies that the rGO/ZnO/anti-EpCAM foam can be used for potential CTC capture device for the clinical blood samples. In short, we believe that this specific recognition and capture capability of hierarchical nanostructured surfaces will be very useful for applications in cell capture, detection, and diagnosis.

In conclusion, we reported a high-yield cancer cell-capture filter based on novel 3D graphene composited foams. We demonstrated that it can successfully capture cancer cells from blood spiked with MCF-7 cells due to the enhanced local topographic interactions between the 3D nanostructured substrates and extracellular extensions, in addition to specific anti-EpCAM/cell adhesion molecule biological recognition. It is conceivable that our filter-like foam can provide a convenient and cost-efficient alternative for CTC sorting in clinics. Integrating microfluidic components on the membrane filter and making it a lab-on-a-chip device for characterization of single cells will be a very powerful tool for cancer research. The impact of this cell capture platform may even go beyond CTC sorting, potentially benefitting the diagnosis of early diseases that are currently being detected by means of cell-capture technologies.

Experimental Section

Preparation of Free-Standing Reduced Graphene Oxide Composite Foam (rGO/ZnO Foam): Graphene oxide (GO) was prepared from natural graphite powder (Sigma, 45 µm) via a modified Hummers method.[52,53] Upon obtaining the GO water suspension, the nickel foam (NF) was used as a template for the fabrication of the graphene foam. The NF sheets (diameter: 1.5 cm) were immersed in a GO suspension (C_{GO} = 2.2 mg/mL). The NF containing GO suspensions were subsequently transferred into the autoclave, with 10 µL hydrazine monohydrate

added. Next, the autoclave was heated at 90 °C for 16 h to obtain the reduced rGO/NF. The removal of NF from the rGO/NF was performed by immersing rGO/NF in hydrochloric acid (2 mol/L) at 80 °C for 10 h before keeping it at room temperature overnight. Finally, the released rGO foam was rinsed and dialyzed several times with deionized water to remove residual acid and metal ions. The ZnO nanorods were prepared via a modified method from literature;[54] specifically, grown in aqueous solution containing 25 mM zinc nitrate hydrate and 25 mM hexamethylenetetramine (HMTA), at 90 °C for 6 h.

Binding of Biotinylated Anti-EpCAM to rGO/ZnO Foam (rGO/ZnO/Anti-EpCAM Foam): 3-Aminopropyl-tris(trimethylsiloxy)-silane (ATTS), a kind of amine-functionalized silane, was deposited onto rGO/ZnO foam by the vacuum vapour method. The cleaned substrates were placed in an air-tight desiccator containing one drop of ATTS. The desiccator was set under vacuum conditions for 2 h. As a consequence, the ATTS molecules were organized in a layer with their free amino groups away from the substrate. 1 mM sulfosuccinimidyl 6-(4′-azido-2′-nitrophenylamino) hexanoate (sulfo-SANPAH) in 50 mM HEPES (pH 8.5) was applied onto the nanostructured graphene foam under UV (365 nm) light illumination for 12 min, after which the foam was washed with 50 mM HEPES (pH 8.5) 2 times before use. The foam was further treated with 10 μg/mL of streptavidin (SA) in PBS solution for 30 min at room temperature,[26] leading to its immobilization onto the foam (Supporting Information, session 2), before being flushed with PBS to remove excess SA. After binding the SA onto the foam, 25 μL biotinylated anti-EpCAM (10 μg/mL in PBS with 1% (w/v) BSA and 0.09% (w/v) sodium azide) was dropped onto the foam and incubated for 30 min before washing with PBS.

Cancer Cell Capturing Test: The rGO/ZnO/anti-EpCAM foam was placed in a suitable chamber, into which 1 mL of cell suspension (10^5 cells/mL) was loaded. After incubating the device setup for 30 min at 37 °C and 5% CO_2, the substrate was gently washed with PBS for at least 5 times. The captured cells were fixed with 4% PFA in PBS for 20 min, followed by further treatment with 0.2% Triton X-100 in PBS for 10 min. The captured cells were then stained by DAPI for 5 min. The number of captured cell could be estimated by recording the number of clear blue dots (staining with DAPI, blue fluorescence) represented cells on focal plane and indistinct dots represented cells at different focal planes that are out of focus (Figure S3). By constructing the 3D images from the images of different confocal planes, which were at the same xy observation position, we could count the number of the cells at one observation position.

Electrical Measurements of rGO/ZnO/Anti-EpCAM Foam During CTCs Capturing: We put the rGO/ZnO/anti-EpCAM foam on glass substrate, and built a incubated chamber, and then we use Pt wire as the electrodes. We use the epoxy glue to encapsulate the part of Pt wires which was in the DMEM (as shown in Figure 3a). The rGO/ZnO/anti-EpCAM foam was incubated in 0.1% Tween 20 for 1h before measurement, to passivate uncoated graphene area. In order to compare with the optical microscopy results, the density of and MCF7 cell was determined to be 10^5 cells/mL. All electrical measurements were conducted in DMEM under 37 °C and 5% CO_2 (schematic drawing of the devices shown in Figure 3a) using a semiconductor characterization system (Keithley 4200-SCS).

Cancer Cell Capture from the Artificial CTC Blood Sample: For ease of detection, MCF7 were stained with red fluorescent dye (CellTracker™ Red CMTPX (Ex/Em: 577/602 nm)) before being spiked into the blood samples. The artificial CTC-containing blood samples were prepared by spiking 10 mL mouse (C57BL/6) blood with pre-stained MCF7 cells, such that the final MCF7 cell concentration would be between 2000–2200 cells/mL. Male and female C57BL/6 mice ranging from ages eight to ten-weeks old were allowed to acclimate in the animal housing area for about one week before experimentation. During this acclimation period, animals were fed a standard diet and allowed unlimited access to food and water. All mice received humane care in accordance with the Guide for the Care and Use of Laboratory Animals. All the procedures were carried on under standard laboratory conditions at room temperature, 22 °C. Blood samples were collected from heart, in succession from anesthetized mice. The plunger of the needle was then gently aspirated as to collect as much blood from each cardiac cycle as possible and not collapse the heart. Using this technique, approximately 0.7 to 1.0 mL of blood was collected. The collection of blood samples from all the sampling sites on each animal was carried on in less than seven minutes by assistance of two technicians, and the blood samples were processed in K3-EDTA tubes with 8–10 times inversion for analysis, immediately after blood was collected. After that, cell suspension was loaded into a syringe (as shown in Figure S5), which is connected to the top of rGO/ZnO/anti-EpCAM foam directly. Another empty syringe was connected to the bottom of rGO/ZnO/anti-EpCAM foam chamber. Sample was dispensed to traverse through the foam filter manually by pushing the plunger of the top syringe. The flow-through was collected by the bottom syringe. After the sample has been passed through the rGO/ZnO/anti-EpCAM foams, the number of CTCs with fluorescent labelling could be readily counted by using flow cytometry (BD LSRII). Table S1 summarizes the number of red blood cells, white blood cells and platelets (obtained by Beckman Coulter AC.T DiffTM Analyzer) of fresh mouse (C57BL/6) blood which passed through the rGO/ZnO/anti-EpCAM foam. As shown in Table S1, the number of red blood cells, white blood cells and platelets in fresh blood does not change significantly before and after passed through the rGO/ZnO/anti-EpCAM foam. This implies that the rGO/ZnO/anti-EpCAM foam is with good biocompatibility and can be used for potential CTC capture device for the clinical blood samples.

For flow cytometry experiment, stained cells were analyzed with Accurri on Dickinson (BDTM) LSRII flow cytometer. Analysis of flow cytometry results were performed with Flowjo software. For CTC detection, cells with fluorescent staining were analysis analyzed by flow cytometry (LSR II from BD Biosciences). Results were analyzed by the Flowjo software.

Supporting Information

Supporting Information is available from the Wiley Online Library or from the author.

Acknowledgements

This work was supported by the Singapore National Research Foundation (NRF-RF2009–04 and CREATE Programme of Nanomaterials for Energy and Water Management).

Received: September 22, 2013
Revised: November 15, 2013
Published online: December 19, 2013

[1] K. S. Novoselov, A. K. Geim, S. V. Morozov, D. Jiang, M. I. Katsnelson, I. V. Grigorieva, S. V. Dubonos, A. A. Firsov, *Nature* **2005**, *438*, 197–200.
[2] A. K. Geim, K. S. Novoselov, *Nat. Mater.* **2007**, *6*, 183–191.
[3] X. Huang, Z. Yin, S. Wu, X. Qi, Q. He, Q. Zhang, Q. Yan, F. Boey, H. Zhang, *Small* **2011**, *7*, 1876–1902.
[4] H. Chen, M. B. Müller, K. J. Gilmore, G. G. Wallace, D. Li, *Adv. Mater.* **2008**, *20*, 3557–3561.
[5] S. Park, N. Mohanty, J. W. Suk, A. Nagaraja, J. An, R. D. Piner, W. Cai, D. R. Dreyer, V. Berry, R. S. Ruoff, *Adv. Mater.* **2010**, *22*, 1736–1740.
[6] Q. Ji, I. Honma, S.-M. Paek, M. Akada, J. P. Hill, A. Vinu, K. Ariga, *Angew. Chem. Int. Ed.* **2010**, *49*, 9737–9739.
[7] K. Yang, J. Wan, S. Zhang, B. Tian, Y. Zhang, Z. Liu, *Biomaterials* **2012**, *33*, 2206–2214.
[8] H. Hong, K. Yang, Y. Zhang, J. W. Engle, L. Feng, Y. Yang, T. R. Nayak, S. Goel, J. Bean, C. P. Theuer, T. E. Barnhart, Z. Liu, W. Cai, *ACS Nano* **2012**, *6*, 2361–2370.
[9] L. Feng, L. Wu, X. Qu, *Adv. Mater.* **2013**, *25*, 168–186.

[10] H. J. Yoon, T. H. Kim, Z. Zhang, E. Azizi, T. M. Pham, C. Paoletti, J. Lin, N. Ramnath, M. S. Wicha, D. F. Hayes, D. M. Simeone, S. Nagrath, *Nat. Nanotechnol.* **2013**, *8*, 735–741.
[11] S. Yin, Z. Niu, X. Chen, *Small* **2012**, *8*, 2458–2463.
[12] N. Li, Q. Zhang, S. Gao, Q. Song, R. Huang, L. Wang, L. Liu, J. Dai, M. Tang, G. Cheng, *Sci. Rep.* **2013**, *3*, 1604.
[13] K. Sakakibara, J. P. Hill, K. Ariga, *Small* **2011**, *7*, 1288–1308.
[14] S. Yin, Y. Goldovsky, M. Herzberg, L. Liu, H. Sun, Y. Zhang, F. Meng, X. Cao, D. D. Sun, H. Chen, A. Kushmaro, X. Chen, *Adv. Funct. Mater.* **2013**, *23*, 2972–2978.
[15] K. Pantel, R. H. Brakenhoff, B. Brandt, *Nat. Rev. Cancer* **2008**, *8*, 329–340.
[16] M. Yu, S. Stott, M. Toner, S. Maheswaran, D. A. Haber, *J. Cell Biol.* **2011**, *192*, 373–382.
[17] G. P. Gupta, J. Massagué, *Cell* **2006**, *127*, 679–695.
[18] C. L. Chaffer, R. A. Weinberg, *Science* **2011**, *331*, 1559–1564.
[19] S. Maheswaran, L. V. Sequist, S. Nagrath, L. Ulkus, B. Brannigan, C. V. Collura, E. Inserra, S. Diederichs, A. J. Iafrate, D. W. Bell, S. Digumarthy, A. Muzikansky, D. Irimia, J. Settleman, R. G. Tompkins, T. J. Lynch, M. Toner, D. A. Haber, *N. Engl. J. Med.* **2008**, *359*, 366–377.
[20] S. Balasubramanian, D. Kagan, C. J. Hu, S. Campuzano, M. J. Lobo-Castañon, N. Lim, D. Y. Kang, M. Zimmerman, L. Zhang, J. Wang, *Angew. Chem. Int. Ed.* **2011**, *50*, 4161–4164.
[21] E. I. Galanzha, E. V. Shashkov, T. Kelly, J.-W. Kim, L. Yang, V. P. Zharov, *Nat. Nanotechnol.* **2009**, *4*, 855–860.
[22] M. Hosokawa, T. Hayata, Y. Fukuda, A. Arakaki, T. Yoshino, T. Tanaka, T. Matsunaga, *Anal. Chem.* **2010**, *82*, 6629–6635.
[23] I. Desitter, B. S. Guerrouahen, N. Benali-Furet, J. Wechsler, P. A. Jänne, Y. Kuang, Y. Masahiko, L. Wang, J. A. Berkowitz, R. J. Distel, Y. Cayre, *Anticancer Res.* **2011**, *31*, 427–441.
[24] S. J. Tan, R. L. Lakshmi, P. Chen, W.-T. Lim, L. Yobas, C. T. Lim, *Biosens. Bioelectron.* **2010**, *26*, 1701–1705.
[25] S. Hou, L. Zhao, Q. Shen, J. Yu, C. Ng, X. Kong, D. Wu, M. Song, X. Shi, X. Xu, W.-H. Ouyang, R. He, X.-Z. Zhao, T. Lee, F. C. Brunicardi, M. A. Garcia, A. Ribas, R. S. Lo, H.-R. Tseng, *Angew. Chem. Int. Ed.* **2013**, *52*, 3379–3383.
[26] S. Nagrath, L. V. Sequist, S. Maheswaran, D. W. Bell, D. Irimia, L. Ulkus, M. R. Smith, E. L. Kwak, S. Digumarthy, A. Muzikansky, P. Ryan, U. J. Balis, R. G. Tompkins, D. A. Haber, M. Toner, *Nature* **2007**, *450*, 1235–1239.
[27] S. L. Stott, C.-H. Hsu, D. I. Tsukrov, M. Yu, D. T. Miyamoto, B. A. Waltman, S. M. Rothenberg, A. M. Shah, M. E. Smas, G. K. Korir, F. P. Floyd, A. J. Gilman, J. B. Lord, D. Winokur, S. Springer, D. Irimia, S. Nagrath, L. V. Sequist, R. J. Lee, K. J. Isselbacher, S. Maheswaran, D. A. Haber, M. Toner, *Proc. Natl. Acad. Sci. USA* **2010**, *107*, 18392–18397.
[28] J. Chen, J. Li, Y. Sun, *Lab Chip* **2012**, *12*, 1753–1767.
[29] J. Sekine, S.-C. Luo, S. Wang, B. Zhu, H.-R. Tseng, H.-h. Yu, *Adv. Mater.* **2011**, *23*, 4788–4792.
[30] S. Wang, K. Liu, J. Liu, Z. T. F. Yu, X. Xu, L. Zhao, T. Lee, E. K. Lee, J. Reiss, Y.-K. Lee, L. W. K. Chung, J. Huang, M. Rettig, D. Seligson, K. N. Duraiswamy, C. K. F. Shen, H.-R. Tseng, *Angew. Chem. Int. Ed.* **2011**, *50*, 3084–3088.
[31] T. Gervais, J. El-Ali, A. Gunther, K. F. Jensen, *Lab Chip* **2006**, *6*, 500–507.
[32] S. Wang, H. Wang, J. Jiao, K.-J. Chen, G. E. Owens, K.-i. Kamei, J. Sun, D. J. Sherman, C. P. Behrenbruch, H. Wu, H.-R. Tseng, *Angew. Chem. Int. Ed.* **2009**, *48*, 8970–8973.
[33] L. Chen, X. Liu, B. Su, J. Li, L. Jiang, D. Han, S. Wang, *Adv. Mater.* **2011**, *23*, 4376–4380.
[34] H. Liu, X. Liu, J. Meng, P. Zhang, G. Yang, B. Su, K. Sun, L. Chen, D. Han, S. Wang, L. Jiang, *Adv. Mater.* **2013**, *25*, 922–927.
[35] S. Hou, H. Zhao, L. Zhao, Q. Shen, K. S. Wei, D. Y. Suh, A. Nakao, M. A. Garcia, M. Song, T. Lee, B. Xiong, S.-C. Luo, H.-R. Tseng, H.-h. Yu, *Adv. Mater.* **2013**, *25*, 1547–1551.
[36] H. Liu, Y. Li, K. Sun, J. Fan, P. Zhang, J. Meng, S. Wang, L. Jiang, *J. Am. Chem. Soc.* **2013**, *135*, 7603–7609.
[37] I. M. Feigel, H. Vedala, A. Star, *J. Mater. Chem.* **2011**, *21*, 8940–8954.
[38] T. A. Yap, S. K. Sandhu, P. Workman, J. S. de Bono, *Nat. Rev. Cancer* **2010**, *10*, 514–523.
[39] Q. Shen, L. Xu, L. Zhao, D. Wu, Y. Fan, Y. Zhou, W.-H. Ouyang, X. Xu, Z. Zhang, M. Song, T. Lee, M. A. Garcia, B. Xiong, S. Hou, H.-R. Tseng, X. Fang, *Adv. Mater.* **2013**, *25*, 2368–2373.
[40] X. Jiang, D. A. Bruzewicz, A. P. Wong, M. Piel, G. M. Whitesides, *Proc. Natl. Acad. Sci. USA* **2005**, *102*, 975–978.
[41] A. K. Shalek, J. T. Robinson, E. S. Karp, J. S. Lee, D.-R. Ahn, M.-H. Yoon, A. Sutton, M. Jorgolli, R. S. Gertner, T. S. Gujral, G. MacBeath, E. G. Yang, H. Park, *Proc. Natl. Acad. Sci. USA* **2010**, *107*, 1870–1875.
[42] S. T. Kim, D.-J. Kim, T.-J. Kim, D.-W. Seo, T.-H. Kim, S.-Y. Lee, K. Kim, K.-M. Lee, S.-K. Lee, *Nano Lett.* **2010**, *10*, 2877–2883.
[43] G.-S. Park, H. Kwon, D. W. Kwak, S. Y. Park, M. Kim, J.-H. Lee, H. Han, S. Heo, X. S. Li, J. H. Lee, Y. H. Kim, J.-G. Lee, W. Yang, H. Y. Cho, S. K. Kim, K. Kim, *Nano Lett.* **2012**, *12*, 1638–1642.
[44] Z. Li, R. Yang, M. Yu, F. Bai, C. Li, Z. L. Wang, *J. Phys. Chem. C* **2008**, *112*, 20114–20117.
[45] H. Hong, J. Shi, Y. Yang, Y. Zhang, J. W. Engle, R. J. Nickles, X. Wang, W. Cai, *Nano Lett.* **2011**, *11*, 3744–3750.
[46] C. G. Rao, D. Chianese, G. V. Doyle, M. C. Miller, T. Russell, R. A. Sanders, L. Terstappen, *Int. J. Oncol.* **2005**, *27*, 49–57.
[47] J. M. de la Fuente, A. Andar, N. Gadegaard, C. C. Berry, P. Kingshott, M. O. Riehle, *Langmuir* **2006**, *22*, 5528–5532.
[48] Y.-F. Kuo, Y.-Z. Su, Y.-H. Tseng, S.-Y. Wang, H.-M. Wang, P. J. Chueh, *Free Radical Biol. Med.* **2010**, *49*, 214–226.
[49] IyerS, R. M. Gaikwad, V. Subba Rao, C. D. Woodworth, I. Sokolov, *Nat. Nanotechnol.* **2009**, *4*, 389–393.
[50] K. E. Fischer, B. J. Aleman, S. L. Tao, R. H. Daniels, E. M. Li, M. D. Bunger, G. Nagaraj, P. Singh, A. Zettl, T. A. Desai, *Nano Lett.* **2009**, *9*, 716–720.
[51] W. J. Allard, J. Matera, M. C. Miller, M. Repollet, M. C. Connelly, C. Rao, A. G. J. Tibbe, J. W. Uhr, L. W. M. M. Terstappen, *Clin. Cancer Res.* **2004**, *10*, 6897–6904.
[52] S. Park, R. S. Ruoff, *Nat. Nanotechnol.* **2009**, *4*, 217–224.
[53] W. S. Hummers, R. E. Offeman, *J. Am. Chem. Soc.* **1958**, *80*, 1339–1339.
[54] L. E. Greene, M. Law, J. Goldberger, F. Kim, J. C. Johnson, Y. Zhang, R. J. Saykally, P. Yang, *Angew. Chem. Int. Ed.* **2003**, *42*, 3031–3034.